Insights into the pores of the microwave-assisted synthesized metal-imidazolate frameworks showing enhanced gas sorption

Suvendu Sekhar Mondal,[a] Subarna Dey,[b] Ahmed G. Attallah,[c,d] Reinhard Krause-Rehberg,[c] Christoph Janiak,[b] and Hans-Jürgen Holdt[a],*

[a]Institut für Chemie, Anorganische Chemie, Universität Potsdam, Karl-Liebknecht-Straße 24-25, 14476 Potsdam, Germany; E-mail: holdt@uni-potsdam.de

[b]Institut für Anorganische Chemie und Strukturchemie, Heinrich-Heine-Universität Düsseldorf, 40204 Düsseldorf, Germany

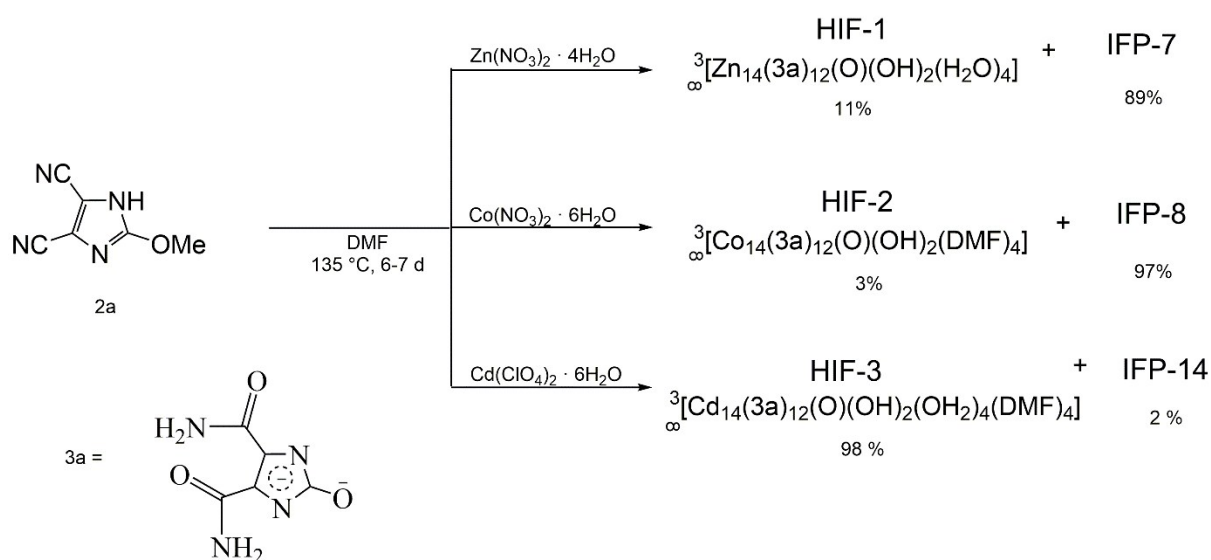[c]Institut für Physik, Martin-Luther-Universität Halle-Wittenberg, Von-Danckelmann-Platz 3, 06120 Halle, Germany

[d]Physics Department, Faculty of Science, Minia University, P.O. 61519, Egypt

Supporting Information

(19 pages)

CONTENTS

Reaction scheme:

2a →(DMF, 135 °C, 6-7 d)

Zn(NO$_3$)$_2$ · 4H$_2$O → HIF-1 $^3_\infty$[Zn$_{14}$(3a)$_{12}$(O)(OH)$_2$(H$_2$O)$_4$] 11% + IFP-7 89%

Co(NO$_3$)$_2$ · 6H$_2$O → HIF-2 $^3_\infty$[Co$_{14}$(3a)$_{12}$(O)(OH)$_2$(DMF)$_4$] 3% + IFP-8 97%

Cd(ClO$_4$)$_2$ · 6H$_2$O → HIF-3 $^3_\infty$[Cd$_{14}$(3a)$_{12}$(O)(OH)$_2$(OH$_2$)$_4$(DMF)$_4$] 98 % + IFP-14 2 %

Percentage (%) of yield and material formation at different conditions.

	IFP-7	HIF-1	IFP-8	HIF-2	IFP-14	HIF-3[1]
CE-condition (DMF; 135 °C and 6-7 d)	89	11	97	3	2	98
MW-assisted conditions (DMF, 120 °C, 60 min)	100	0	100	0	0	100

Scheme S1. Schematic presentation of the synthesis of IFP and hydrogen-bonded MBB structure denoted as HIF.
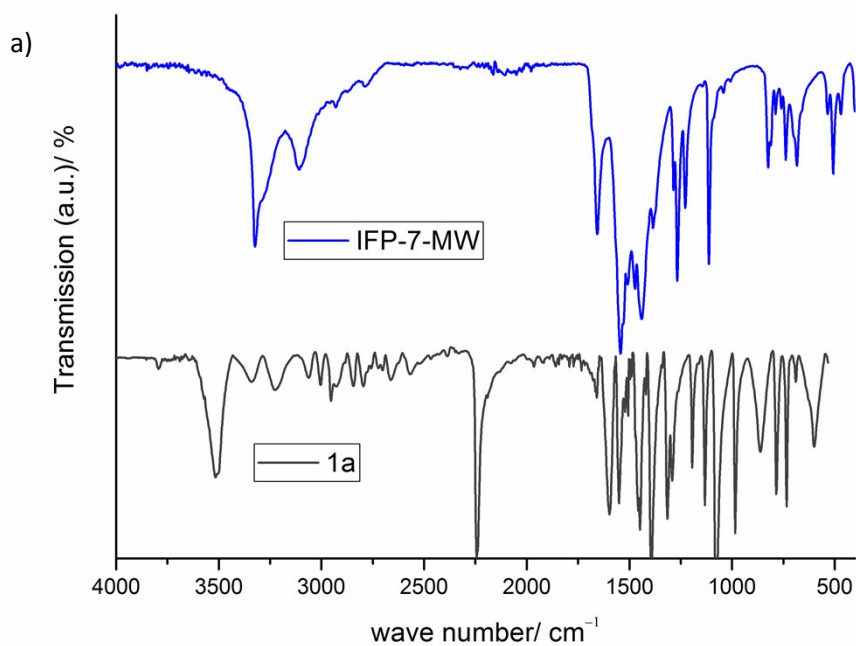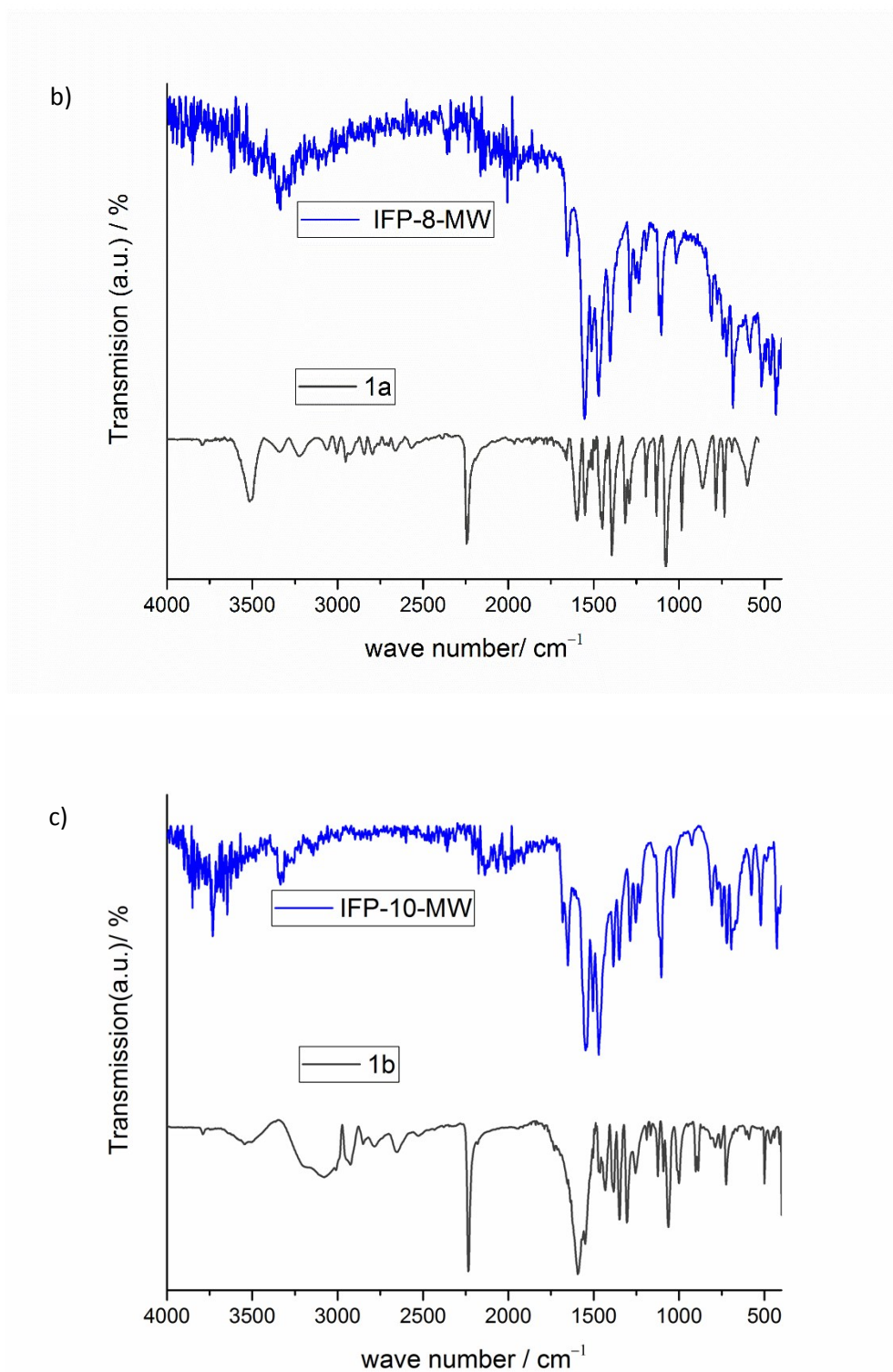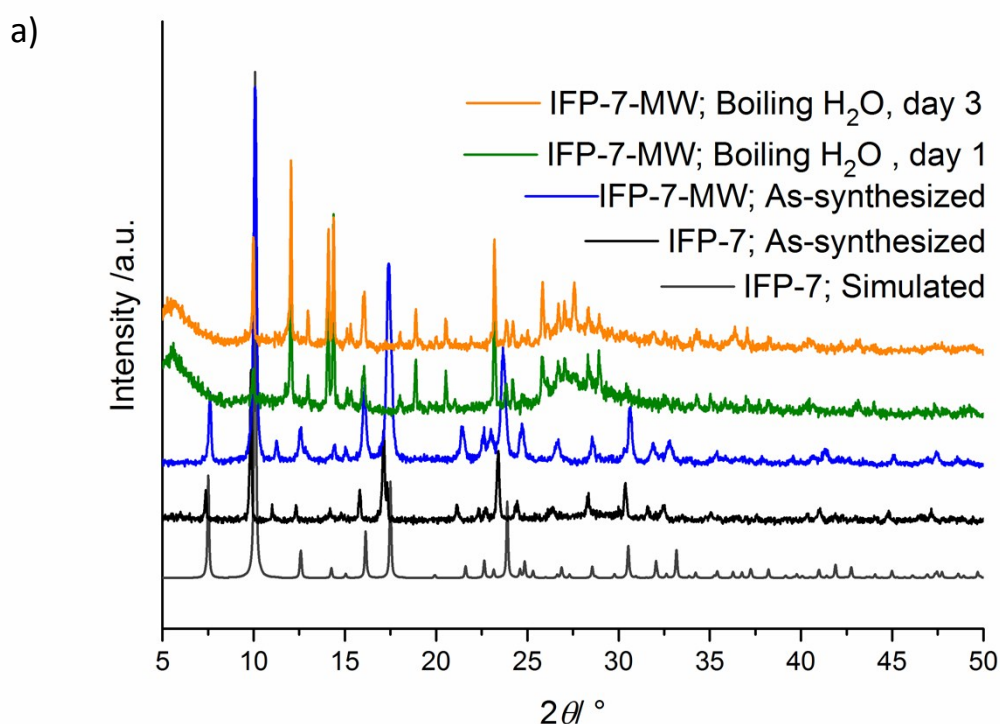
Figure S1. IR-spectra of: a) as-synthesized IFP-7-MW and 4,5- dicyano-2-methoxyimidazole (1a); b) as-synthesizedIFP-8-MW and 4,5- dicyano-2-methoxyimidazole (1a); c) as-synthesized IFP-10-MW and 4,5-dicyano-2-ethoxyimidazole (2a).
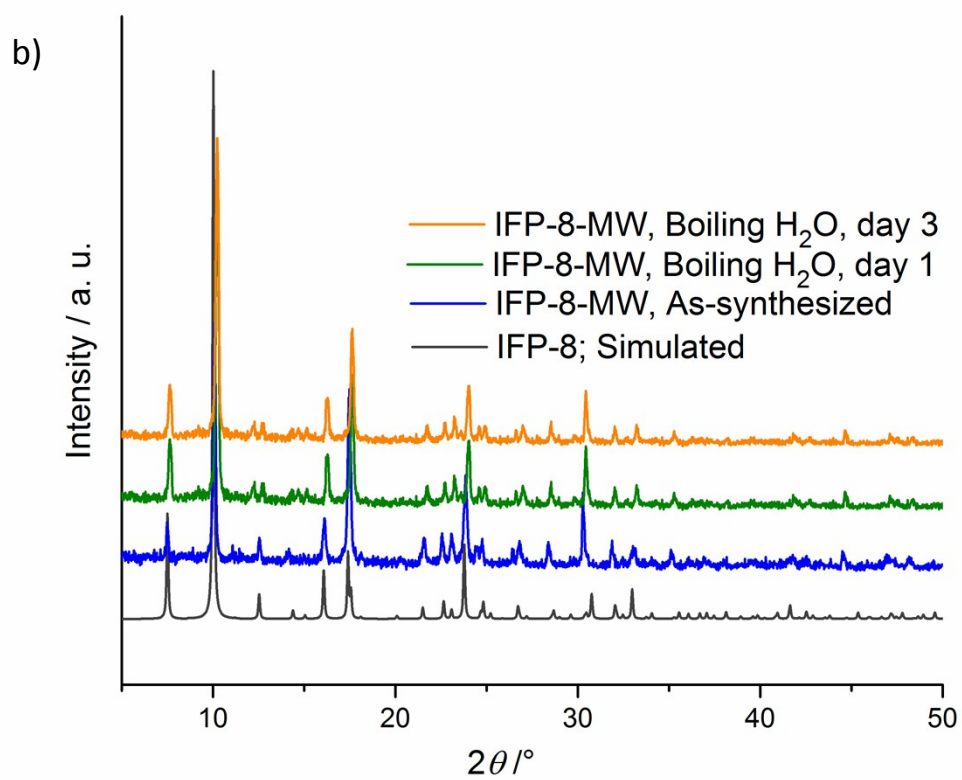
The degree of in situ hydrolysis of the cyano groups of 1a (or 1b) into the corresponding linker 2a (or 1b) was studied with infrared (IR) spectroscopy. The IR-spectra manifested no stretching bands related to C≡N in the region of 2205–2225 cm^{-1} (Figure S1). Instead, new typical bands for amide and imidate groups were observed at around 1550 cm^{-1} and 1660 cm^{-1}. Among other prominent IR

changes, those associated with N−H resonances were noticeable. Centered at 3320 cm^{-1}, a broad amide N−H band with considerable fine structure was noted.

Powder X-ray diffraction (PXRD)

For X-ray powder patterns of IFPs were measured on a Siemens Diffractometer D5005 in Bragg-Brentano reflection geometry. The Diffractometer was equipped with a copper tube, a scintillation counter, with stepper motor controlled variable slits on both primary and diffracted beams (automatical incident- and diffracted-beam soller slits) and with a graphite secondary monochromator. The generator was set to 40 kV and 40 mA with using Cu K-alpha radiation (1.54056 Å). All measurements were performed with sample rotating. Data were collected digitally from 3° to 70° 2ϑ using a step size of 0.02° 2ϑ and a count time of 4 seconds per step.

a)

Intensity /a.u.

— IFP-7-MW; Boiling H$_2$O, day 3
— IFP-7-MW; Boiling H$_2$O , day 1
— IFP-7-MW; As-synthesized
— IFP-7; As-synthesized
— IFP-7; Simulated
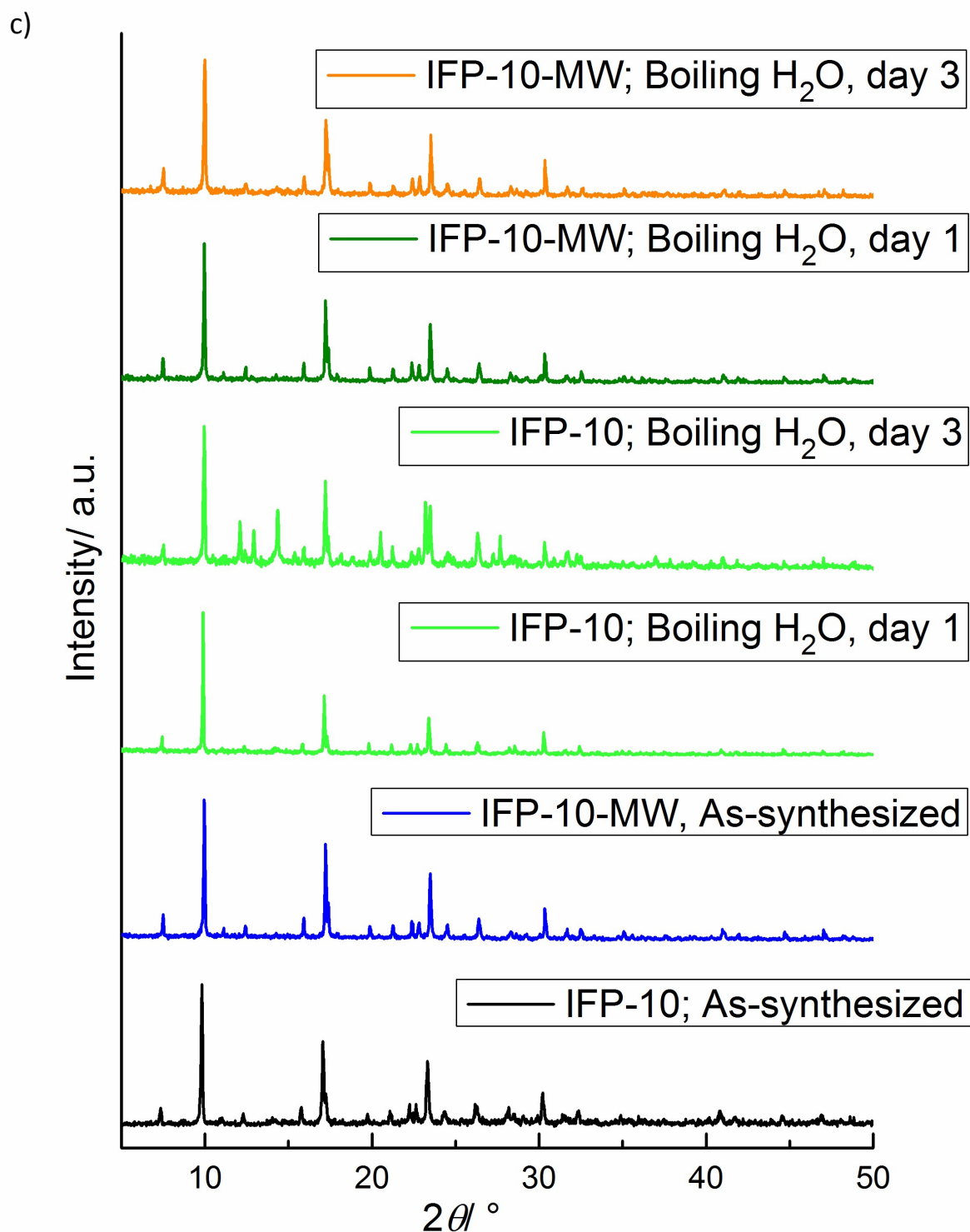
2θ/ °

b)

c)

Figure S2. Powder X-ray diffraction profiles of IFP, collected during stability tests in refluxing water.

Scanning electron microscopy

SEM measurements was done on a JEOL JSM 6510 SEM. For measurements all samples were activated under vacuum by 200 °C for 24 h and then coated with carbon (POLARON CC7650 Carbon Coater).

Gas-sorption measurements

Sorption isotherms were measured using a Micromeritics ASAP 2020 automatic gas sorption analyzer equipped with oil-free vacuum pumps (ultimate vacuum <10^{-8} mbar) and valves, which guaranteed contamination free measurements. The sample was connected to the preparation port of the sorption analyzer and degassed under vacuum until the out gassing rate, i.e., the rate of pressure rise in the temporarily closed manifold with the connected sample tube, was less than 2 µTorr/min at the specified temperature 60 °C for 24 h. After weighing, the sample tube was then transferred to the analysis port of the sorption analyzer. All used gases (H_2, He, N_2, and CO_2) were of ultra-high purity (UHP, grade 5.0, 99.999%) and the STP volumes are given according to the NIST standards (293.15 K, 101.325 kPa). Helium gas was used for the determination of the cold and warm free space of the sample tubes. H_2 and N_2 sorption isotherms were measured at 77 K (liquid nitrogen bath), whereas CO_2 sorption isotherms were measured at 273.15 K (ice/deionized water bath).
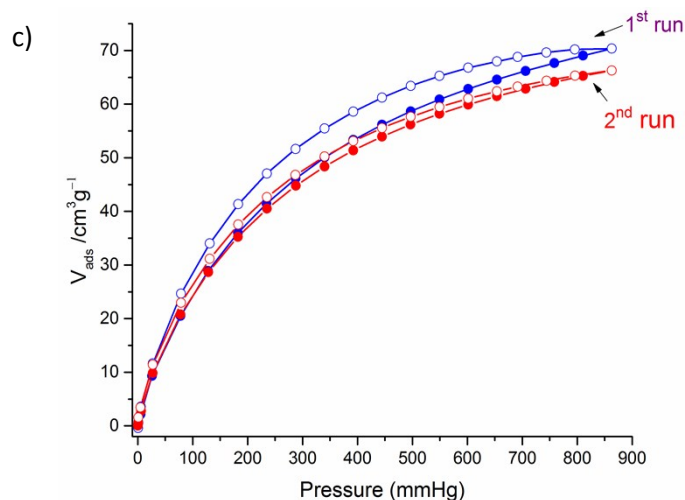
c)
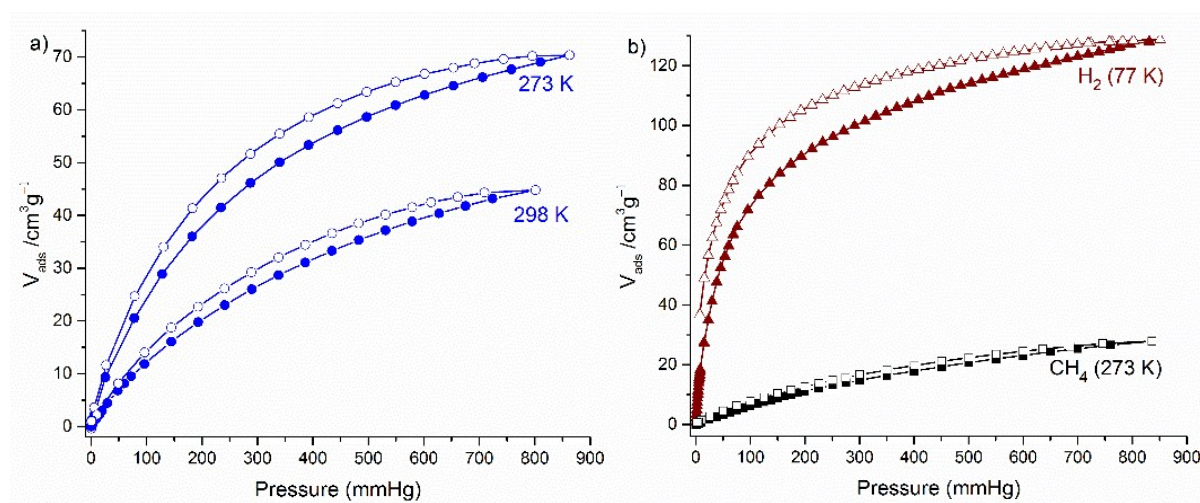
Figure S3. Gas sorption isotherms for activated IFP-7-MW, a) CO_2; b) H_2 and CH_4; (c) Gas sorption isotherms for activated IFP-7-MW, for CO_2 at 273 K for 2nd run. Adsorption and desorption branches are indicated by closed and open symbols, respectively.
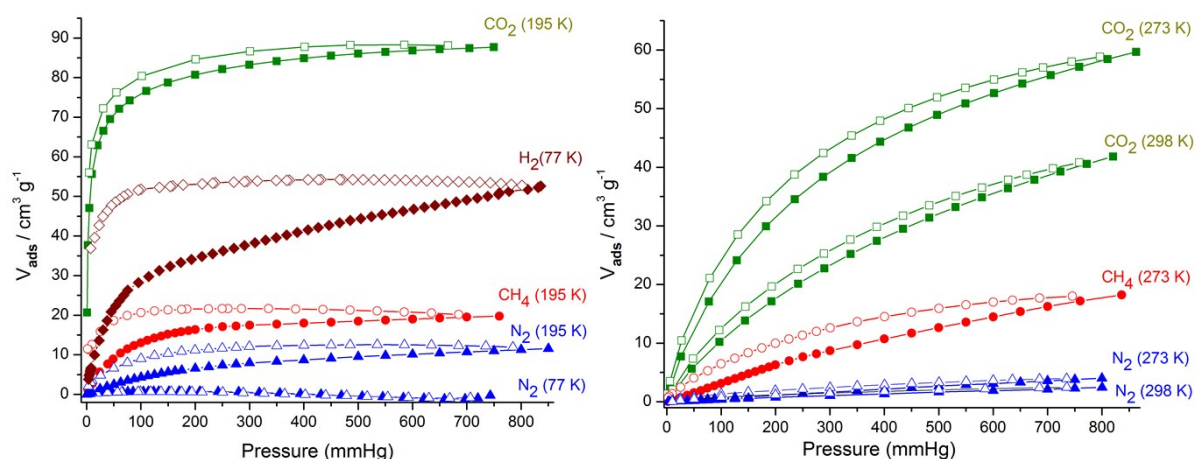

Figure S4. Gas sorption isotherms for activated IFP-7-CE. Adsorption and desorption branches are indicated by closed and open symbols, respectively. Images are reproduced from Holdt et al., *Chem. Commun.,* 2013, **49**, 7599−7601.

The origin of the broad H_2 desorption hysteresis was raised by one of the Referees when we submitted our IFP-7 manuscript at *ChemComm* (Holdt et al., *Chem. Commun.,* 2013, **49**, 7599−7601). According to the previous Referee's suggestion, we did further experiments with increased equilibrium time for H_2 and CO_2 gas-sorption isotherms of IFP-7-CE. The results are reproduced here from the ESI of that *ChemComm* paper. Results indicated that similar kinds of hysteresis for both (H_2 and CO_2) at desorption isotherms are observed as mentioned in the ESI (see Figure S5, Figure S7 and Table S1 for details). This also tells the reproducibility of the gas sorption properties regarding in the capacity and moreover the kinetic behaviour. Therefore, we can suggest that the methoxy group has flexibility and gate-opening behavior. Additionally, we did further H_2 gas sorption experiment with IFP-1(IFP-1 is isostructural to IFP-7 but with a methyl group instead of methoxy; Figure S6) that was published previously (*Angew. Chem. Int. Ed.,* 2010, **49**, 1258–1262). For IFP-1, the H_2 uptake amount was reported to 1.5 wt% and no hysteresis was noted. In our instrument (same measurement condition as for IFP-7-CE) H_2 uptake capacity of IFP-1 shows again the same result and no hysteresis is observed (see Fig. S5 for details). This direct comparison of isostructural materials differing only a methyl vs methoxy substituent (Figure S6) is a further strong evidence of the flexibility of methoxy

group and its action in the gate opening behavior of IFP-7. We found one literature that MOFs having alkyl ether side chains can act as a molecular gate due to the chain's flexibility. Fischer and co-workers have reported a honeycomb-like zinc-dicarboxylate-bipyridine framework with flexible alkyl ether side chains (S. Henke and R. A. Fischer, *J. Am. Chem. Soc.* 2011, **133**, 2064–2067). Such framework shows gate-effects based on gas sorption (N_2, CO_2 and CH_4) measurements. The CO_2 sorption measurements of that material at 195, 273, and 298 K show typical type I isotherms with high gas uptake capacity. At 195 K, a steep increase of the CO_2 uptake observed in the low-pressure region and a small hysteresis is visible in the desorption branch. The hysteresis can be attributed to slow kinetics of desorption as they reported. In our article, we presented a hexagonal zinc-organic framework with flexible methoxy substituents. Such framework showed gas sorption (N_2, CO_2 and CH_4) behavior similar to the zinc-dicarboxylate-bipyridine framework with flexible alkyl ether side chains.

Mentioned below is reproduced from Holdt et al., *Chem. Commun.,* 2013, **49**, 7599−7601

Table S1 summarizes the equilibrium time interval, measurement time and H_2 uptake for IFP-7-CE. The H4 type hysteresis is mostly caused by irreversible uptake of molecules in pores (or through pore entrances). [(a) K. S. W. Sing, D. H. Everett, R. A. W. Haul, L. Moscou, R. A. Pierotti, J. Rouquerol and T. Siemieniewska, *Pure Appl. Chem.*, 1985, **57**, 603-619; (b) M. Thommes, B. Smarsly, M. Groenewolt, P. I. Ravikovitch, A. V. Neimark, *Langmuir* 2005, **22**, 756-764.]. We have increased the equilibration interval up to 50 s which had taken the measurement time 68 h. If we further increased the equilibration interval, then it will be a problem to keep the temperature constant (77 K).

Table S1. H_2 uptake measurements at different equilibrium time interval for IFP-7-CE.

Condition		Curve or Experiment	Measurement time (h)	H_2 uptake (cm³/g) [a]
Absolute pressure (mmHg)	Equilibration Interval [b] (s)			
0-50	20			
50-500	15	curve or experiment 1	IFP-7: 29 IFP-1: 8	35
500-1000	10			
0-50	30			
50-500	30	curve or experiment 2	38	37
500-1000	30			
0-50	50			
50-500	50	curve or experiment 3	68	50
500-1000	50			

[a] H_2 uptake with a standard deviation of ±15 cm³/g at 77 K and 1 bar.
[b] Equilibration time allowed during both adsorption and desorption at each data point up in the stated pressure range
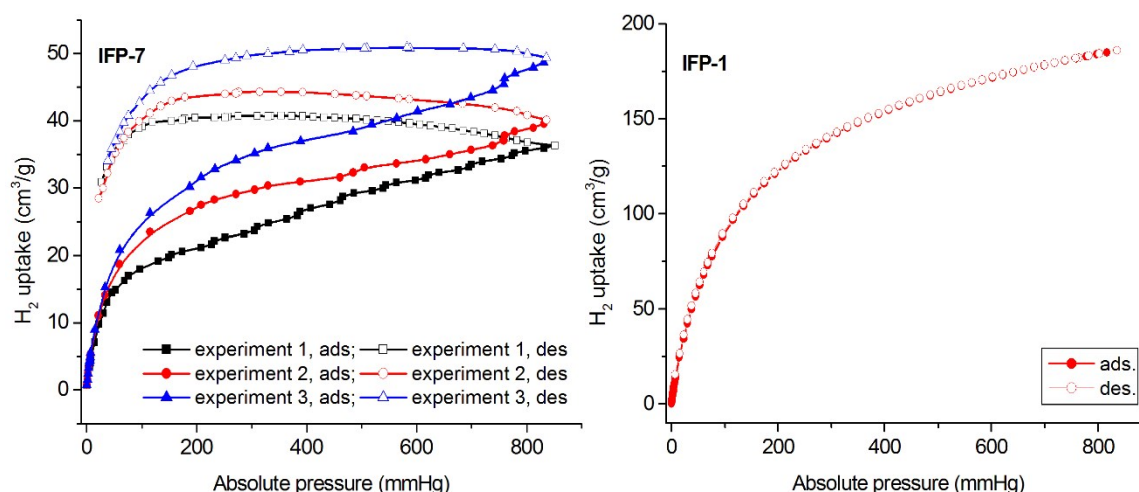
Figure S5. H_2 gas sorption isotherms of IFP-7-CE under different equilibration interval. (left) and IFP-1 (right). Adsorption and desorption branches are indicated in closed and open symbols, respectively.

To compare the hysteresis of IFP-7-CE, we measured the H_2 sorption at a similar condition (curve or exp.-1) for IFP-1 which is isostructural to IFP-7-CE except for the methyl instead of a methoxy group (IFP-1 contains a *methyl* group; IFP-7 contains a *methoxy* group, Figure S6). In IFP-1, there is no hysteresis during the desorption (Fig. S9, right). Therefore, we confirmed that the equilibrium time interval is not a key issue for such broad hysteresis.
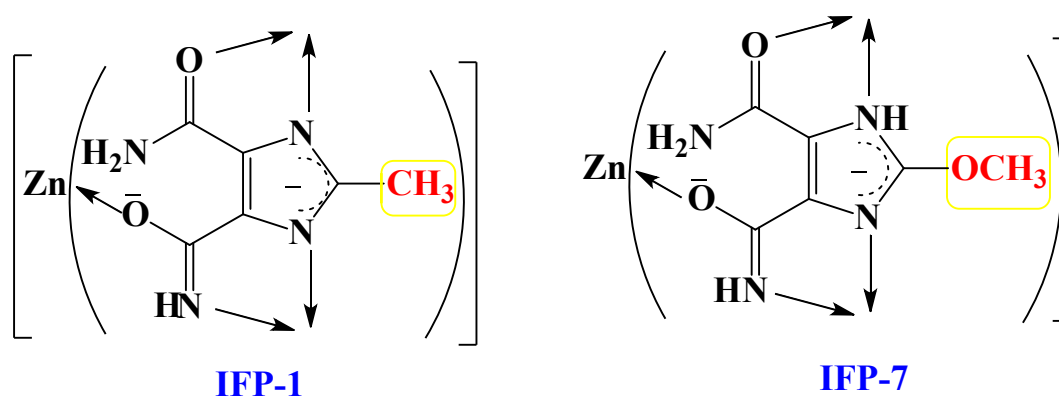
Figure S6. Schematic structure of IFP-1 (left) and IFP-7 (right)

The broad desorption hysteresis for H_2 in IFP-7-CE does not change with the equilibrium time interval. This was also confirmed for the narrower desorption hysteresis of CO_2 at 273 K in IFP-7-CE. At 273 K, again we observed the similar hysteresis when the ad- and desorption equilibrium time interval was increased to 30 s over the whole pressure (Figure S7).
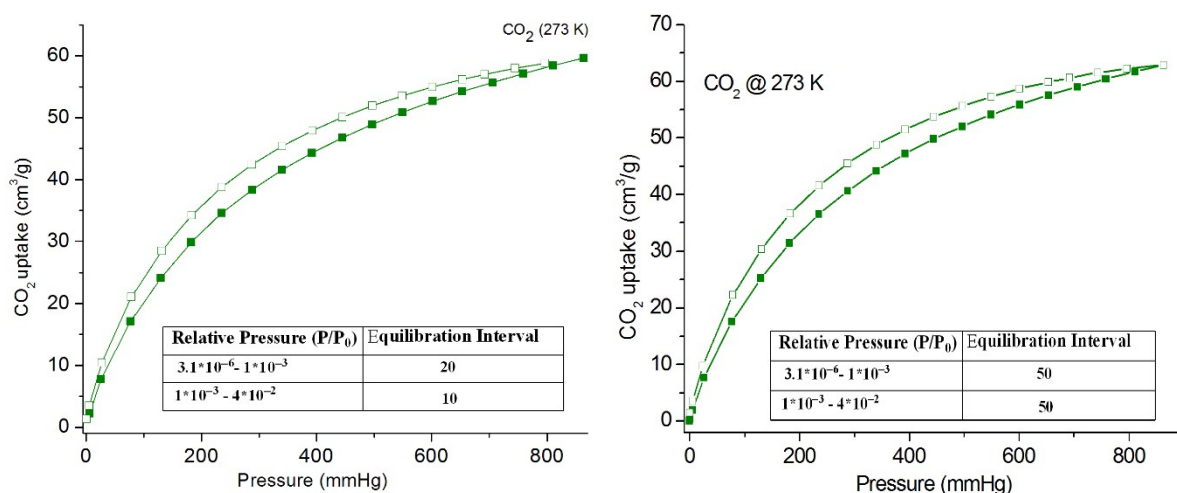
Figure S7. CO_2 gas sorption isotherms of IFP-7-CE under different equilibration interval, showing almost no change in hysteresis upon desorption.
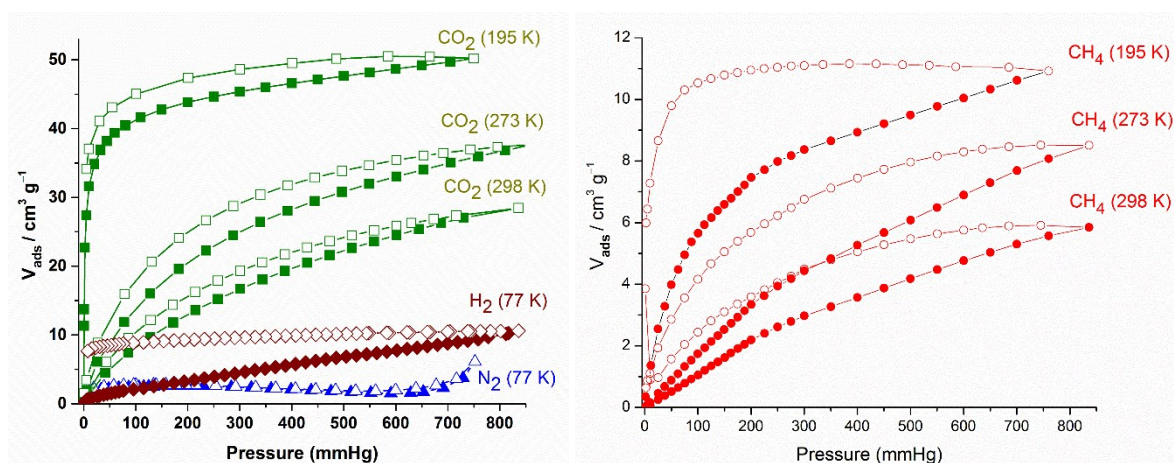

Figure S8. Gas sorption isotherms for activated IFP-8-CE. Adsorption and desorption branches are indicated by closed and open symbols, respectively. Images are reproduced from Holdt et al., *Chem. Commun., 2014, **50**, 5441–5443.*

The flexibility is due to the flexible substituent which does not affect the overall structure. However, the framework is very much robust. For example, we have previously shown that XRD pattern after CH_4 uptake for IFP-8 maintained crystalline integrity and peak shifting was not observed (Holdt et al.,*Chem. Commun.*, 2014, **50**, 5441–5443).
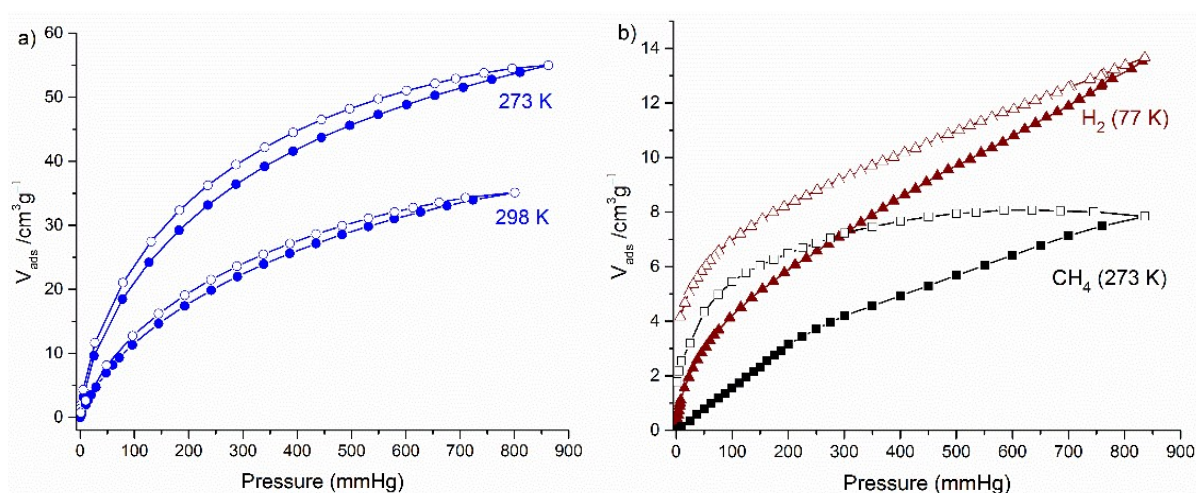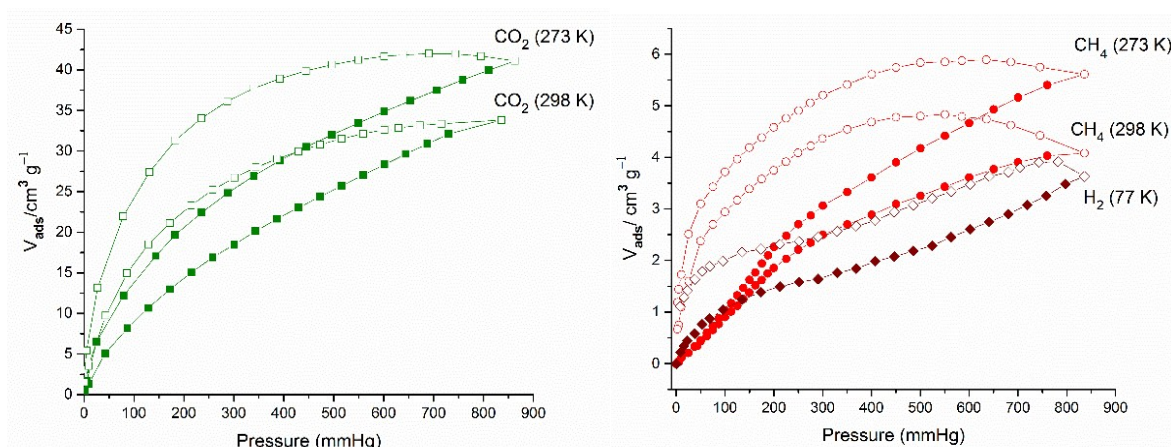
Figure S9. Gas sorption isotherms for activated IFP-10-MW, a) CO_2; b) H_2 and CH_4. Adsorption and desorption branches are indicated by closed and open symbols, respectively.

Figure S10. Gas sorption isotherms for activated IFP-10-CE. Adsorption and desorption branches are indicated by closed and open symbols, respectively. Images are reproduced from *CrystEngComm, 2013, **15**, 9394−9399.*

Heat of adsorption

From two adsorption isotherms acquired at different temperatures T_1 and T_2, the differential heat of adsorption $\Delta H_{ads,diff}$, that is isosteric heat of adsorption Q_{st} can be calculated for any amount of adsorbed substance after determining the required relative pressures p_1 and p_2. A modified form of the Clausius-Clapeyron equation is used (eq. below).[2] $\Delta H_{ads,diff}$ was calculated over the whole adsorption range from the 273 K and 298 K isotherms for CO_2.

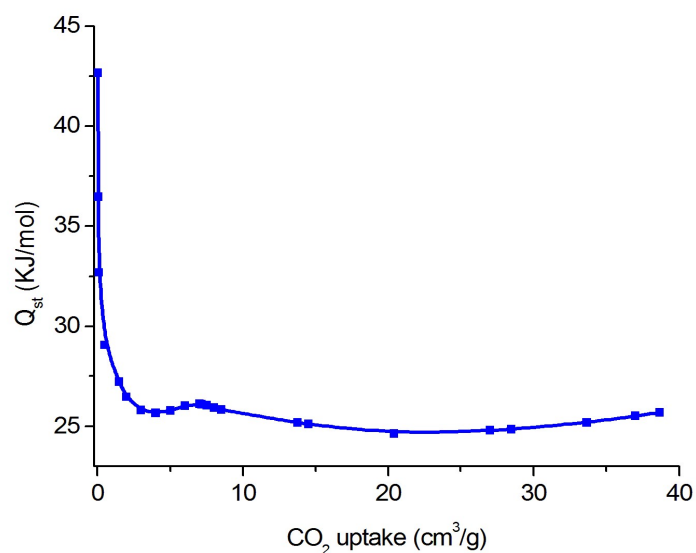$$\Delta H_{ads,diff} = Q_{st} = -Rln\left(\frac{p_2}{p_1}\right)\frac{T_1 T_2}{T_2 - T_1}$$

Figure S11. Isosteric heats of CO_2 adsorption as a function of the adsorbent loading for IFP-7-CE. Image is reproduced from Holdt et al., *Chem. Commun.,* 2013, **49**, 7599–7601.
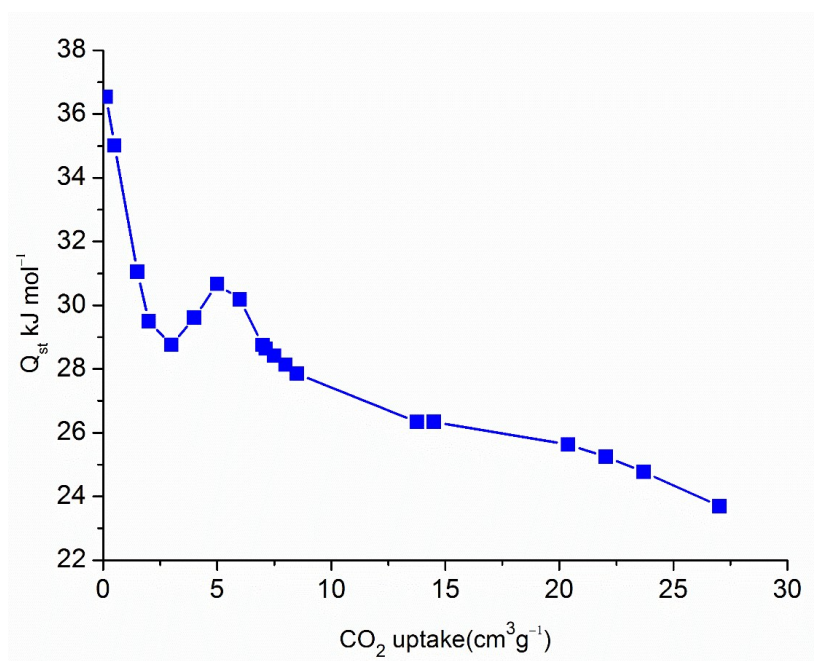

Figure S12. Isosteric heats of CO_2 adsorption as a function of the adsorbent loading for IFP-8-CE. Image is reproduced from Holdt et al., *Chem. Commun., 2014, 50, 5441–5443.*

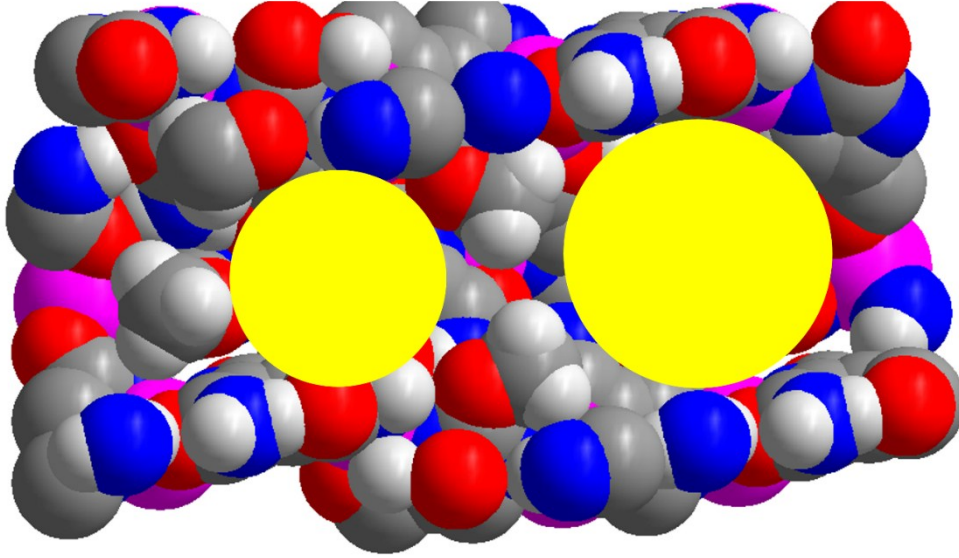**Figure S13.** Two types of pore sizes of IFP-8 (average size: 0.80±0.10 nm; deviation due to flexible group).

Positron Annihilation Lifetime Spectroscopy

Digital Positron Lifetime Spectrometer

The sample was measured at first in air at RT to see the activation effect on the pore size. The samples were annealed isothermally at 200 °C for periods of 3, 6, 9, 12 hrs at each temperature then the measurements were performed at RT. All measurements were performed upon reaching RT after annealing. We used a 7 µCi 22-Na positron source. Two 40 mm x 22 mm EJ232 plastic scintillators coupled to two Hamamatsu PMTs were used. The system gave one resolution function with 225 ps full width at half maximum. A pre and a turbo pumps used to evacuate the samples. A digital positron annihilation spectroscopy, with two Hamamatsu photomultiplier tubes with two plastic scintillator of φ40mm x 22mm dimension and 240 ps resolution (fwhm), was used for these measurements. LT 10 program was used for the LT analysis. The pore size was calculated by using Excited Energy Levels and Various Shapes (EELViS) program,[3,4] and the program depends on the Extended Tao-Eldrup model with the following equation:[5]

$$\lambda_{RTE}(D,T) = \lambda_A - \frac{\lambda_S - \lambda_{3\gamma}}{4}\left[1 - \frac{2\delta}{D} + \frac{\sum_{i=1}^{\infty}\frac{1}{i\pi}\sin\left(\frac{2i\pi\delta}{D}\right)e^{\left(\frac{-\beta i^2}{D^2 kT}\right)}}{\sum_{i=1}^{\infty}e^{\left(\frac{-\beta i^2}{D^2 kT}\right)}}\right]^3 \quad \dots\dots\dots\dots\dots 1$$
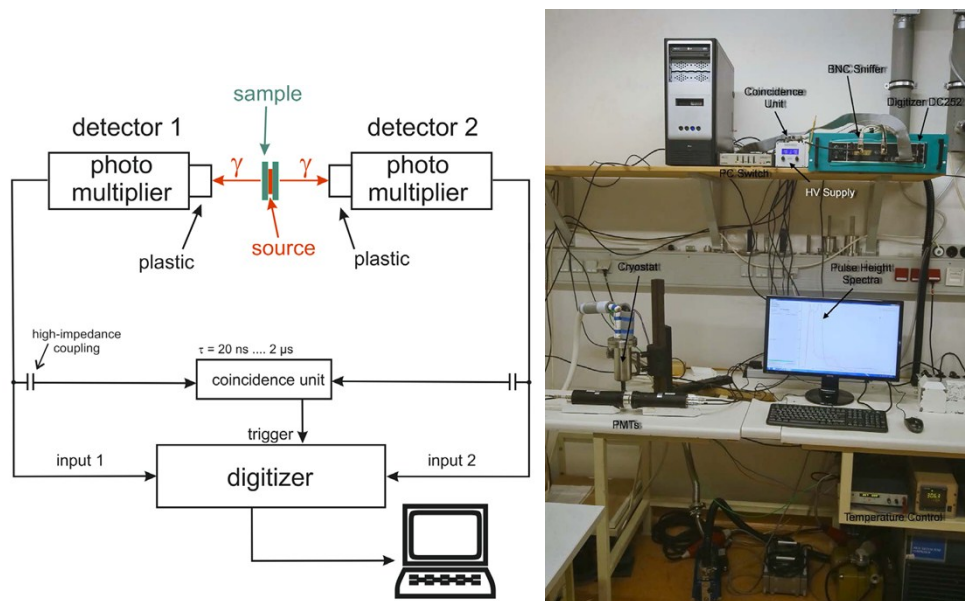
Figure S14. Instrumental set up of digital positron lifetime spectrometer. We used Na^{22} as a positron source and its activity is 7 μCi.
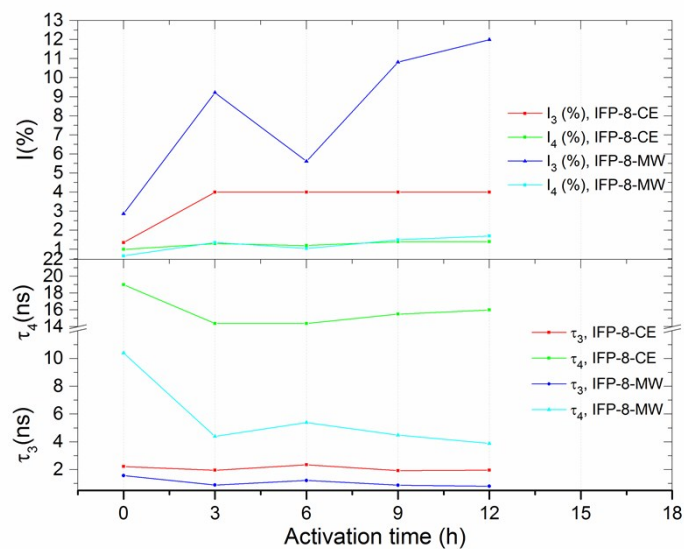

Figure S15. Positron lifetime and intensity of IFP-8 at different annealing temperatures as a function of annealing time.
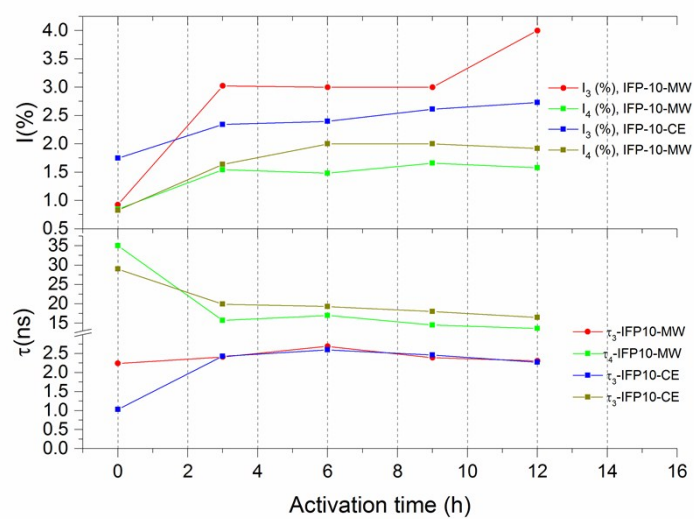
Figure S16. Positron lifetime and intensity of IFP-10 at different annealing temperatures as a function of annealing time.
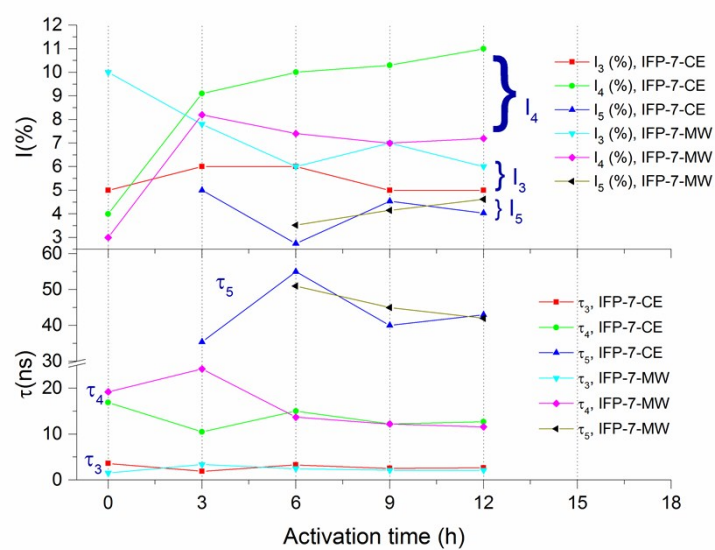

Figure S17. Positron lifetime and intensity of IFP-7 at different annealing temperatures as a function of annealing time.
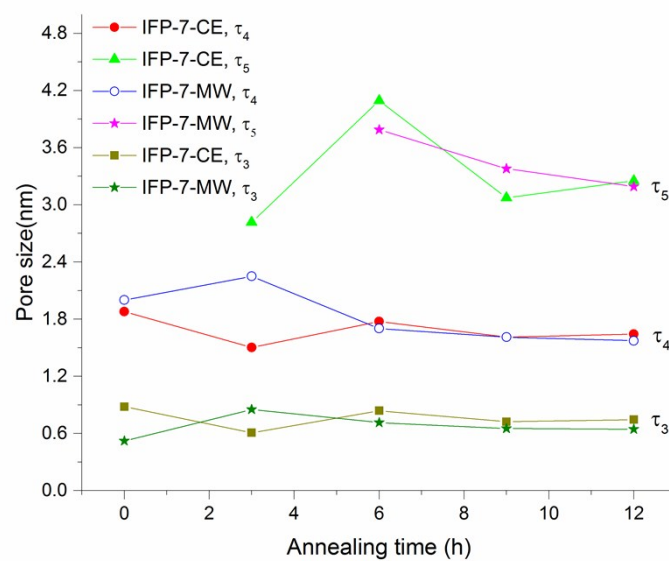
Figure S18. Pore sizes for IFP-7 as a function of annealing time (only the largest pore sizes (τ_5) have standard deviations. points without standard deviation mean that their error values (in positron lifetime) are so small and cannot be used as pore size/deviation).

Thermogravimetric analysis

TG measurements were performed in a static air atmosphere from room temperature to 900 °C with a Perkin Elmer TGA 4000 thermal analyzer. We have presented up to 450 °C. The heating rate was 10 °C min^{-1}. The samples were placed in ceramic pans.
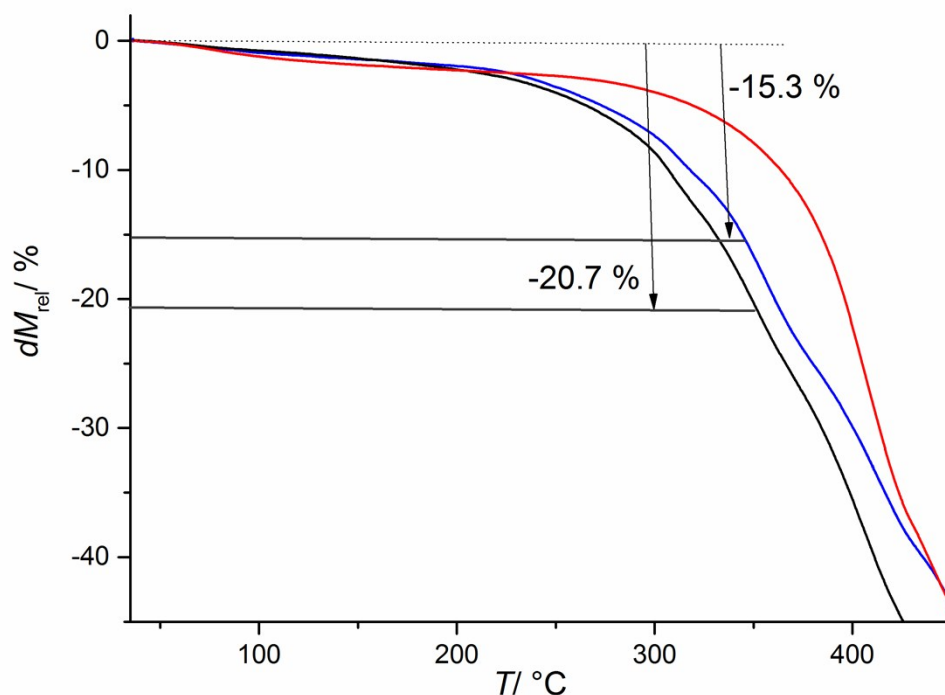
Figure S19. TGA curves for IFP-10 (black: as-synthesized at CE-conditions; blue: as-synthesized at MW-conditions and red: activated at MW-conditions).

References

1   S. S. Mondal, S. Dey, A. G. Attallah, A. Bhunia, A. Kelling, U. Schilde, R. Krause-Rehberg, C. Janiak and H.-J. Holdt, *ChemistrySelect,* 2016, **1**, 4320–4325.

2   F. Rouquerol, J. Rouquerol and K. Sing, *Adsorption by powders and porous solids*, (F. Rouquerol, J. Rouquerol, K. Sing, Eds.), Academic Press, San Diego, 1999, vol. **11**.

3   R. Zaleski, J. Wawryszczuk and T. Goworek, *Radiat. Phys. Chem.,* 2007, **76**, 243−247.

4   http://sourceforge.net/projects/eelvis/

5   D. W. Gidley, T. L. Dull, W. E. Frieze, J. N. Sun and A. F. Yee, *J. Phys. Chem.* B, 2001, **105***, 4657−4662.